ESTIMATION SCHEMES TO EVALUATE ELASTIC-PLASTIC J AND COD FOR THROUGHWALL CIRCUMFERENTIALLY CRACKED ELBOW UNDER CLOSING MOMENT

J.Chattopadhyay*, A.K.S.Tomar, B.K.Dutta and H.S.Kushwaha
Reactor Safety Division, Hall-7
Bhabha Atomic Research Centre
Mumbai – 400085, India
*Email: jchatt@apsara.barc.ernet.in, Phone: +91-22-25591522, Fax: +91-22-25505151

Abstract

Leak-before-break (LBB) assessment of primary heat transport piping of nuclear reactors involves detailed fracture assessment of pipes and elbows with postulated throughwall cracks. Fracture assessment requires the calculation of elastic-plastic *J*-integral and crack opening displacement (COD)[1] for these piping components. Analytical estimation schemes to evaluate elastic-plastic *J*-integral and COD simplify the calculations. These types of estimation schemes are available for pipes with various crack configurations subjected to different types of loading. However, no such schemes are available for throughwall circumferentially cracked elbow (or pipe bend), an important component for LBB analysis. In this paper, simple *J* and COD estimation schemes are proposed for throughwall circumferentially cracked elbow subjected to closing bending moment. The ovalisation of elbow cross section has a significant bearing on its fracture behavior. Therefore, unlike conventional deformation theory plasticity analysis, incremental flow theory is adopted considering both material and geometric non-linearities in the development of the proposed estimation schemes. Although it violates Ilyushin's theorem, it has been shown that the resulting estimation schemes is still reasonably accurate for engineering purposes. Finally, experimental/numerical validation has been provided by comparing the *J*-integral and COD between numerical/test data and predictions of the proposed estimation schemes.

Keywords: Estimation schemes, *J*-integral, Crack opening displacement, Elbow, Pipe Bend, Throughwall circumferential crack

1. Introduction

Leak-Before-Break (LBB) qualification of primary heat transport (PHT) system piping of pressurized heavy water reactor (PHWR, also known as CANDU) or pressurized water reactor (PWR) requires detailed fracture analysis of piping components with postulated throughwall cracks. Since these piping components are mostly made of ductile material, one has to invoke the elastic-plastic fracture mechanics principles to deal with the large-scale plasticity ahead of crack tip. For this purpose, the estimation of elastic-plastic *J*-integral and COD is very essential. Elastic-plastic finite element analysis (FEA) is the most general technique to evaluate these parameters. However, FEA often requires large computational time, expertise and resources, which make the computation quite expensive. Moreover, it has to be carried out on a case-by-case basis for each piping component. To circumvent these problems, simple *J* and COD estimation schemes emerged, first for 2D geometries (Kumar et al, 1981) and then afterwards for pipe geometry with throughwall crack (Kumar et al, 1984) and surface crack (Kumar and German, 1988). All these estimation schemes were based on large number of finite element analysis for a wide range of geometry and material parameters. Non-finite element based estimation schemes were also proposed for throughwall cracked pipes (Klecker et al, 1986, Brust, 1987). Special *J* and COD estimation schemes were also proposed for weld materials by Rahman and Brust (1992). Recently, Kim et al (2002) proposed new *J* and COD estimation schemes or modified the existing schemes for various crack configurations in pipes. Mohan et al (1998) proposed *J* estimation scheme for surface cracked elbow. However, no *J* and COD estimation schemes have appeared in the open literature for throughwall

[1] COD varies along the crack length. It is zero at the crack tips and maximum at the middle. Throughout this paper, COD denotes the maximum crack opening displacement at the middle of crack length.

circumferentially cracked elbows, one of the very important geometry for LBB analyses. The present paper is an effort in that direction. It proposes simple *J* and COD estimation schemes for elbow with throughwall circumferential crack at extrados subjected to in-plane closing bending moment. The basic approach has been same as that of GE/EPRI estimation schemes for pipe with through wall crack under bending moment (Kumar et al, 1984). The following paragraphs describe in detail the methodology followed to develop the proposed scheme and its experimental validation. But, before proceeding with all these details, it is important to understand the unique deformation characteristics of elbow when subjected to bending moment. It has significant influence on the fracture behavior of cracked elbow.

2. Ovalisation of cross section and fracture behavior of elbow

An elbow when subjected to closing bending moment generates tensile stress along the extrados and compressive stress along the intrados (see Fig.1). This, in turn, generates inward components of forces, which try to ovalise the circular cross section of the elbow in such a way that reduces the diameter across the intrados-extrados (across 'a-b' in Fig.1). This pattern of ovalisation tries to stretch the part 'c-d' of the circular cross section of elbow (as shown in Fig.1), which generates a compressive stress field perpendicular to the cross section (i.e. along the axis of the elbow) because of Poisson's contraction. If the crack size at extrados is less than the circumferential length 'cd' (or $2\theta_{th}$ as shown in Fig.1), the crack will be under a compressive normal stress field and will not open up and hence will not cause any weakening of the elbow. Figure 2 depicts the typical axial stress (which is responsible for opening a circumferential crack) variation of a thin (R/t = 20) defect-free elbow subjected to closing bending moment. It is seen from Fig.2 that in the region from extrados extended towards crown (also called flank), axial stress in the thin elbow (R/t = 20) is compressive in nature from $\phi = 180^o$ to almost $\phi = 143^o$ (ϕ indicates the circumferential position at elbow mid-plane). When crack tip falls in the tensile stress field, it starts weakening the elbow. This explains the presence of a threshold crack angle to initiate the weakening. The thicker the elbow, the lower is the threshold crack angle. It has been shown by Chattopadhyay et al (2004a) that the threshold circumferential crack angles, which start weakening an elbow subjected to closing moment, are: $2\theta_{th} = 45^o$, 60^o and 90^o for R/t = 5, 10 and 20 respectively. A qualitative experimental validation of the presence of threshold crack angle to initiate the weakening of elbow has also been shown by Chattopadhyay et al (2005).

Another aspect of the ovalisation of elbow cross section should also be noted. Because of ovalisation as shown in Fig.1, the area moment of inertia of the elbow cross-section with respect to 'SS' axis reduces which, in turn, reduces the bending stiffness during deformation (known as *Geometric Softening*). This expedites the collapse of elbow under closing bending moment.

From the above discussion, it is very clear that any numerical methodology for elbow must capture this ovalisation of cross section to truly represent its deformation characteristics. These aspects have been kept in mind while formulating the methodology in the development of new estimation schemes.

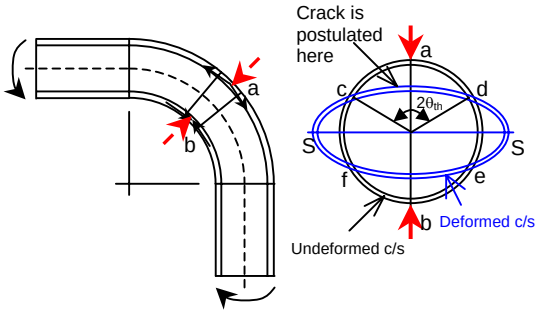

Fig.1 Deformation characteristics of elbow subjected to closing moment

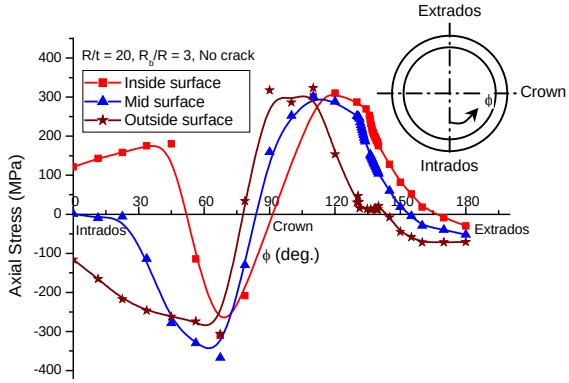

Fig.2 Variation of axial stress at mid-plane of an un-cracked elbow at closing collapse moment

3. Finite element analysis

The finite element method is used to develop the *J* and COD estimation schemes for elbows of various wall thicknesses with different throughwall circumferential crack under in-plane closing bending moment. Finite

element program WARP3D (Gullerud et al, 2002) is used for this study. Non-linear finite element analysis has been carried out to determine *J*-integral and COD of elbows for various geometric and loading combinations. Conventionally, deformation theory plasticity model without considering the geometric non-linearity is adopted to develop the *J* and COD estimation schemes. However, it cannot capture the ovalisation of elbow cross section during its deformation. It has already been mentioned in the preceding section 2 that capturing the ovalisation of elbow cross section is very important to properly model its deformation characteristics. Figure 3 shows the importance of considering geometric non-linearity in the finite element analysis of elbow. Accordingly, incremental flow theory plasticity with consideration of both geometric and material non-linearties is adopted in the present analysis. It violates the Ilyushin's (1946) theorem. However, it will be shown later that the resulting estimation scheme can still be reasonably accurate for engineering purposes. The following sections briefly describe the different aspects of the finite element analysis.

3.1 Geometry

Figure 4 shows the geometry of a throughwall circumferentially cracked (TCC) elbow. The crack is centered at extrados and subjected to closing mode of bending moment. Geometrically, a 90° TCC elbow is characterized by three parameters, namely, R_b/R, R/t and 2θ where, R is the mean cross sectional radius, t is

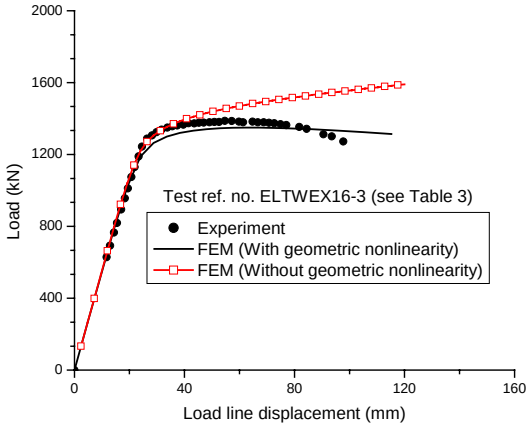

Fig.3 Importance of considering geometric non-linearity: comparison of load-deflection curve

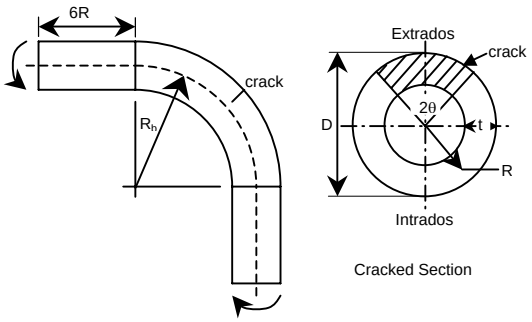

Fig.4 Geometry of a throughwall circumferen-tially cracked elbow under closing moment

the wall thickness, R_b is the mean bend radius at crown and 2θ is the circumferential crack angle. Table 1 shows different combinations of these parameters taken in the study. In general, long radius elbow with $R_b/R = 3$ has been assumed in the present study. However, few short radius elbows with $R_b/R = 2$ have also been analyzed to study the effect of elbow bend radius on estimation schemes. The R/t is varied from 5 to 20 covering a wide range for engineering use. Crack angles (2θ) have been varied from 45° – 150°. A customized pre-processor of NISA (2002) is used to generate the finite element mesh from the given geometry parameters. As mentioned in section 2, there is a threshold crack angle for each R/t. Crack angle below this threshold value does not have any weakening effect on the elbow and the deformation behavior is like a defect-free elbow. Accordingly, the geometry matrix has been chosen as shown in Table 1. In the present analyses, the elbow is connected with straight pipes of length equal to the six times the mean cross sectional radius. It is important to note that this straight pipe length allows free ovalisation propagation from mean elbow section.

Table 1 Various geometric and material parameters of analyzed elbows

R : 250 mm	R : 250 mm
R_b/R : 3	R_b/R : 2
R/t : 5 → 2θ = 45°, 60°, 90°, 120°, 150°	R/t : 5 → 2θ= 45°, 60°, 90°, 120°, 150°
R/t : 7.5 → 2θ = 60°, 90°, 120°, 150°	R/t : 10 → 2θ= 90°, 120°, 150°
R/t : 10 → 2θ = 90°, 120°, 150°	R/t : 20 → 2θ= 120°, 150°
R/t : 15 → 2θ= 120°, 150°	n = 5
R/t : 20 → 2θ= 120°, 150°	No. of cases : 10
n = 3,5,7	
No. of cases : 48	

3.2 Material

Material tensile properties are assumed to follow Hook's law up to yield stress and beyond yield stress, to follow Ramberg-Osgood relation. The equations are as follows:

$$\frac{\varepsilon}{\varepsilon_y} = \frac{\sigma}{\sigma_y} \qquad \text{for } \sigma \le \sigma_y \qquad (1)$$

$$\frac{\varepsilon}{\varepsilon_y} = \frac{\sigma}{\sigma_y} + \alpha\left(\frac{\sigma}{\sigma_y}\right)^n \qquad \text{for } \sigma > \sigma_y \qquad (2)$$

where, σ is the true stress, ε is the true strain, ε_y, σ_y, α and n are the yield strain, yield stress, Ramberg-Osgood coefficient and hardening exponent respectively with $E\varepsilon_y = \sigma_y$, where, E is the Young's modulus. The rationale of not choosing Ramberg-Osgood equation (Eq.(2)) below material yield stress is that it is not realistic. Mohan et al (1998) state that the prediction of the plastic part of J-integral with this material constitutive law is less approximate. The values for some of these parameters have been fixed as: E = 200 GPa, α = 1, σ_y = 300 MPa and ν = 0.3, where, ν is the Poisson's ratio. Later it has been shown that variations of these parameters do not significantly affect the estimation schemes. The Ramberg-Osgood hardening exponent *(n)* has been varied as: n = 3,5,7, which cover a wide range of carbon and stainless steel material.

It should be noted that the Ramberg-Osgood equation (Eq.(2)), although used universally as material constitutive law in estimation schemes, violates the Ilyushin's (1946) theorem. The presence of elastic strain (i.e. the first part of right hand side of Eq.(2)) is the reason behind it. This violation manifests itself in the form of dependences of plastic influence functions (i.e. h_1 for J-integral and h_2 for COD) on load and other material parameters. However, it has been shown later that in spite of these violations, the resulting estimation schemes can still be used for engineering use with reasonable accuracy. Sections 4 and 6 discuss these aspects in more detail.

3.3 Finite Element Model

Twenty-noded solid elements with 3 × 3 × 3 integration order are used to model the elbow. Because of symmetry, only one fourth of the elbow is modeled. There are total 528 elements and 3221 nodes for elbows with extrados crack. Spider web type mesh has been employed near the crack tip for mesh economy. Eight numbers of radial and circumferential divisions have been employed at the spider web with two elements across the thickness of elbow. A very small hole of radius 0.5% of crack length has been introduced at crack tip in the finite element model for faster convergence without much change of results. This was recommended by Kumar et al (1983). Figure 5 shows a typical finite element mesh. The same mesh pattern is used for all the cases. A mesh convergence study has been performed to check the adequacy of this mesh (Fig.6). Additionally, the reasonable path independence of J-integral also confirms the adequacy of the finite element mesh.

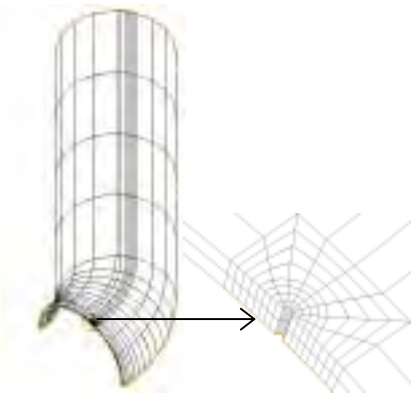

Fig.5 Typical finite element mesh used to model elbow

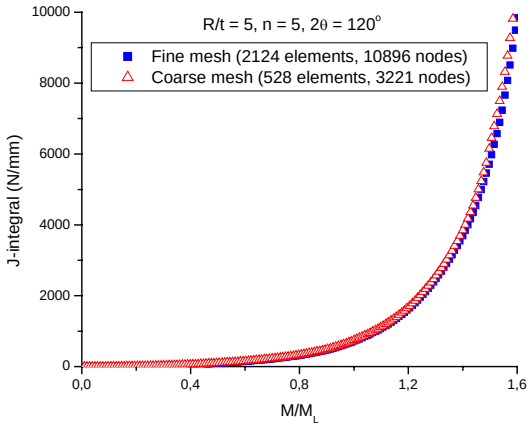

Fig.6 Mesh convergence study : comparison of J-integral

3.4 Loading

In-plane closing bending moment has been applied to the end plane of connecting straight pipe. Bending moment has been simulated as triangularly varying face pressure. However, within an element, face pressure has been kept constant. The face pressure value is obtained as 'M.c/I' where 'M' is the applied bending moment, 'I' is the area moment of inertia of the pipe/elbow cross section and 'c' is the vertical distance of the element face center from the neutral axis. The application of bending moment in this way avoids the spurious plastic deformation at the point of load application.

3.5 Determination of elastic and fully plastic *J*-integral and COD

J-integral values are evaluated by finite element method using the domain integral technique (Shih et al, 1986). In this technique, J-integral is evaluated over a number of contours around the crack tip. In the present study, eight contours are used to obtain the J-integral. However, the first three contours near the crack tip are not considered because of inaccuracy of J-integral values due to very sharp stress and strain gradient. The mean *J*-integral values obtained between 4^{th} – 8^{th} contours are considered. The average *J*-integral along the crack front (i.e. wall thickness) has been calculated as:

$$J_{avg.} = \frac{J_{in} + 4J_{mid} + J_{out}}{6} \tag{3}$$

where, J_{in}, J_{mid} and J_{out} are the *J*-integral at the inside, middle and outside surface node of crack front respectively. Henceforth, *J*-integral would mean average *J*-integral. The COD at inside and outside surface are directly obtained from the FEA output. Once the elastic-plastic *J*-integral and COD are obtained from FEA, the elastic parts of these parameters are subtracted to get the fully plastic *J*-integral and COD.

The elastic *J*-integral for TCC elbow subjected to closing bending moment is obtained using the following equation:

$$J_e = \frac{K^2}{E} \tag{4}$$

where, J_e is the elastic *J*-integral, *K* is the stress intensity factor (SIF) and *E* is the Young's modulus. The SIF for TCC elbow under in-plane bending moment is evaluated as follows (Chattopadhyay et al, 1994):

$$K = A_e \sigma_b \sqrt{\pi a} \tag{5}$$

$$\sigma_b = \frac{M}{\pi R^2 t} \tag{6}$$

$$A_e = \left[\left(C_1 + C_2 h^{p1}\right) + \left(C_3 + C_4 h^{p2}\right)\left(\frac{\theta}{\pi}\right)^{p3} \right] + \left[\left(C_5 + C_6 h^{p4}\right) + \left(C_7 + C_8 h^{p5}\right)\left(\frac{\theta}{\pi}\right)^{p6} \right]\left(\frac{t}{R}\right)^{p7} \tag{7}$$

$C_1 = -3.4628$, $C_2 = 4.446$, $C_3 = -52.429$, $C_4 = 52.445$, $C_5 = -2.2524$, $C_6 = 1.1102$, $C_7 = 0.8634$, $C_8 = 1.7283$, $p_1 = 0.1366$, $p_2 = -0.1848$, $p_3 = 2.6137$, $p_4 = 0.1216$, $p_5 = 0.0695$, $p_6 = 0.4587$, $p_7 = -0.5119$

where, *M* is the bending moment, *R* is the mean radius of cross section, *t* is the wall thickness, $a\ (= R\theta)$ is the semi-crack length, $h\ (= tR_b/R^2)$ is the elbow factor or pipe bend characteristics.

There is no solution available for elastic COD of TCC elbow subjected to closing bending moment. Accordingly, it has been developed here. The basic form of the equation of elastic COD is similar to that proposed by Zahoor (1989-1991) and Kozluk et al (1988) for elbow with throughwall axial crack and is as follows:

$$\delta_e = \frac{4MV_2}{\pi D_o^{\ 2} E} \tag{8}$$

where, D_o is the outer diameter of elbow cross section, V_2 is a parameter which depends on R/t and crack angle (2θ) and other symbols have the same meaning as in the Eqs.(4-6). The V_2 parameter is calculated from the initial few elastic load steps for each geometry. It is calculated separately for COD at inside and outside surface and for all combinations of R/t and 2θ as shown in Table 1.

The plastic component of *J*-integral and COD are obtained from FEA as follows:

$$J_p = J^{FE} - J_e \tag{9}$$

$$\delta_p = \delta^{FE} - \delta_e \tag{10}$$

where, J^{FE} and δ^{FE} are the total *J*-integral and COD respectively obtained from FEA and J_e and δ_e are their elastic components as obtained from Eqs.(4-8). The plastic components of *J*-integral and COD for throughwall circumferentially cracked pipe subjected to bending moment are, in general, expressed as follows (Zahoor,1989-1991):

$$J_p = \alpha\sigma_y\varepsilon_y\pi R\left(1-\frac{\theta}{\pi}\right)^2 h_1\left(\frac{M}{M_L}\right)^{n+1} \tag{11}$$

$$\delta_p = \alpha\varepsilon_y\pi R h_2\left(\frac{M}{M_L}\right)^{n} \tag{12}$$

where, M_L is the limit moment which is proportional to σ_y. α and n are the constants in Ramberg-Osgood Eq.(2). h_1 and h_2 are the non-dimensional plastic influence functions which ideally depend only on R/t, n and 2θ if the conditions of Ilyushin's theorem are not violated.

The same form is retained in this paper for plastic components of *J*-integral and COD for TCC elbow subjected to closing bending. The plastic influence functions (h_1, h_2) are evaluated for each case using the Eqs.(11-12). It will be shown later in section 4 that this form of equation for plastic *J*-integral and COD require some modifications in the α terms to take care of the anomaly in the Ramberg-Osgood equation, which violates Ilyushin's theorem. These modifications, however, will not alter the values of plastic influence functions (h_1, h_2), because these are generated for $\alpha = 1$. The limit moment for TCC elbow subjected to closing bending moment has been recently proposed by Chattopadhyay et al (2004a). The same is used here. The limit moment is expressed as follows (Chattopadhyay et al, 2004a):

$$M_L = M_0.X \tag{13}$$

$$M_0 = 1.075\, h^{2/3}\,(4R^2t\sigma_y) \tag{14}$$

where, M_L and M_0 are the limit moments of cracked and defect-free elbows respectively and *X* is the weakening factor which is a function of crack size (2θ) and the R/t of the elbow as shown in Table 2. It may be recalled from section 2 that there is a threshold throughwall circumferential crack angle to initiate the weakening of elbow subjected to closing bending moment, which is seen from the values of weakening factor *X*.

Table 2 Ao, A1 and A2 values for function X = Ao + A1.(θ/π) + A2.(θ/π)2

R/t	A_o	A_1	A_2	θ limits
5	1.1194	-0.7236	-2.0806	for $45^o \le 2\theta \le 150^o$ and X =1 for $2\theta < 45^o$
7.5	1.1185	-0.3420	-2.5200	for $60^o \le 2\theta \le 150^o$ and X =1 for $2\theta < 60^o$
10	0.9655	1.0152	-4.6800	for $60^o \le 2\theta \le 150^o$ and X = 1 for $2\theta < 60^o$
15	1.1400	0.3000	-3.6000	for $90^o \le 2\theta \le 150^o$ and X = 1 for $2\theta < 90^o$
20	0.6400	3.4200	-7.9200	for $90^o \le 2\theta \le 150^o$ and X = 1 for $2\theta < 90^o$

Table 3 Geometry constants (V2) for COD and plastic influence functions, h1 for J-integral and h2 for COD for various R/t, 2 and n values (Rb/R = 3)

R/t	2θ	V_2 at inner surface	V_2 at outer surface	n	h_2 at inner surface	h_2 at outer surface	h_1
5	45^0	5.5654	5.9672	3	0.3962	0.4023	0.4319
				5	0.4514	0.4765	0.4596
				7	0.4859	0.5246	0.4874
	60^0	8.5567	10.3962	3	0.6020	0.7333	0.7971
				5	0.6873	0.8418	0.8661
				7	0.7165	0.8718	0.8884
	90^o	19.9227	25.9920	3	1.3164	1.6581	1.9881
				5	1.5600	1.9188	2.2707
				7	1.6384	1.9829	2.3241
	120^o	42.4302	53.947	3	1.6349	1.9636	2.3755
				5	1.9651	2.3178	2.9852
				7	1.8504	2.1587	2.7601
	150^o	82.8908	100.9991	3	1.4122	1.6256	1.7667
				5	1.3851	1.5860	1.9418
				7	1.2622	1.4368	1.7474
7.5	45^0	4.67	3.24	3	0	0	0
				5	0	0	0
				7	0	0	0
	60^0	7.9881	7.8352	3	0.2807	0.2320	0.2843
				5	0.3186	0.3616	0.3919
				7	0.2418	0.2683	0.2283
	90^o	24.2572	28.7168	3	0.9543	1.1273	1.3194
				5	1.0773	1.2686	1.4388
				7	0.6306	0.7374	0.7882
	120^o	62.5898	73.7440	3	1.3057	1.4897	1.7757
				5	1.5340	1.7252	2.1194
				7	0.8555	0.9598	1.1656
	150^o	135.8948	155.2898	3	1.3728	1.4961	1.5124
				5	1.4742	1.6150	1.9535
				7	0.8121	0.8883	1.0976
10	60^0	0	0	3	0	0	0
				5	0	0	0
				7	0	0	0
	90^o	22.9689	24.6002	3	0.6964	0.7718	0.8883
				5	0.7839	0.8993	0.9847
				7	0.7351	0.8301	0.9894
	120^o	79.0440	88.5720	3	1.5654	1.7361	2.2238
				5	1.4777	1.6153	2.0474
				7	1.3576	1.4712	1.8670
	150^o	193.0767	211.9581	3	1.4967	1.6014	1.8571
				5	1.3597	1.4547	1.7351
				7	1.0918	1.1615	1.3267
15	90^o	0	0	3	0	0	0
				5	0	0	0
				7	0	0	0
	120^o	90.7464	93.2147	3	1.1961	1.2741	1.6903
				5	1.3485	1.4292	1.8693
				7	1.2595	1.3174	1.8657
	150^o	305.9804	320.0995	3	1.7154	1.7855	2.4374
				5	1.5433	1.6066	2.0967
				7	1.3084	1.3567	1.7067
20	90^o	0	0	3	0	0	0
				5	0	0	0
				7	0	0	0
	120^o	62.9593	54.6570	3	1.0187	1.0583	1.4895
				5	1.1927	1.2278	1.8537
				7	1.4639	1.5118	2.1961
	150^o	397.2191	401.8272	3	1.8465	1.8899	3.0360
				5	1.8800	1.9248	2.8713
				7	2.0465	2.1035	2.9916

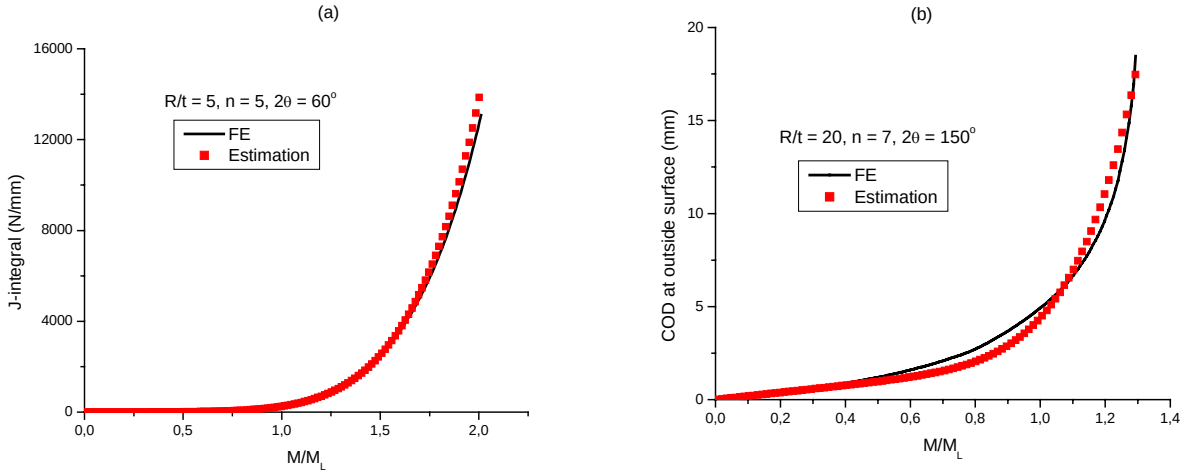

Fig.7 Comparison of (a) J-integral and (b) COD between finite element results and estimation scheme predictions for one typical case. Same pattern is observed in other cases also.

4. Proposed *J* and COD estimation schemes

The geometry constants (V_2 in Eq.(8)) to evaluate elastic COD at inside and outside surface and also the plastic influence functions i.e. h_1 for *J*-integral and h_2 for COD at inside and outside surface in Eqs.(11-12) are evaluated for various geometric cases and Ramberg-Osgood hardening index, n = 3,5,7. The results are shown in Table 3. Linear interpolation may be done to obtain h_1, h_2 and V_2 for any intermediate values of R/t, 2θ and n. The presence of threshold crack angle for each R/t value is again emphasized here. It should be noted that the plastic influence functions are ideally dependent only on R/t, 2θ and n and independent of load, α, σ_y or any other parameters, provided the conditions of Ilyushin's theorem are satisfied. However, the conditions are violated in the present study because of various considerations : i) The presence of elastic strain in Ramberg-Osgood equation (i.e. presence of first term in the right hand side of Eq(2)), ii) the consideration of geometric changes during deformation. Because of these violations, the plastic influence functions show load dependence. These plastic influence functions show very strong load dependence during the initial elastic loading phase and saturates to almost constant value at higher load ($M/M_L > 1$). However, this load dependence of plastic influence functions does not really affect the *J* and COD estimation schemes because, at initial elastic load level, the contribution of plastic component in the total *J*-integral/COD is insignificant and later at higher load when the plastic contribution becomes significant, the plastic influence functions saturate. Figure 7 shows one typical case where it is seen that predictions of *J* and COD estimation schemes and the finite element values are quite close in spite of the load dependence of the plastic influence functions. The problem is much more serious with the dependence on α terms. It was pointed out by several researchers (Zahoor, 1987, Piping Review Committee, 1984, Novtech Corporation, 1988) that the plastic *J*-integral using the Eq.(11) is highly over-predicted when compared with test data. Zahoor (1987) showed that the over-prediction may be as high as 3-7 times the experimental values. Although Zahoor (1987) attributed this to the inconsistency of *J*-estimation equation with respect to the HRR solution, the main reason lies with the form of the material constitutive law. The plastic *J*-integral and COD is proportional to the Ramberg-Osgood coefficient α if only, the material constitutive law is assumed as follows:

$$\frac{\varepsilon}{\varepsilon_y} = \alpha\left(\frac{\sigma}{\sigma_y}\right)^n \qquad (15)$$

However, the Ramberg-Osgood equation (Eq.(2)) contains also the elastic strain term, which is the main reason behind this over-prediction of plastic *J*-integral (and also the COD), especially when the fully plastic state is not attained. It should also be noted that this problem gets masked if one choose α = 1, which is indeed the case for all finite element based estimation schemes. Real materials, in general, exhibit wide range of α = 1-20. Therefore, when one uses the estimation schemes to compare the predictions with the test data for real materials, excessive

over-prediction is observed. To circumvent this problem, Zahoor (1987) proposed to modify the equation to predict the plastic *J*-integral (Eq.(11)) as follows:

$$J_p = \alpha^{\frac{1}{n+1}} \sigma_y \varepsilon_y \pi R \left(1 - \frac{\theta}{\pi}\right)^2 h_1 \left(\frac{M}{M_L}\right)^{n+1} \tag{16}$$

Although, Zahoor (1987) did not mention anything about the COD, but, he did mention that the crack tip opening displacement (CTOD) is proportional to $\alpha^{1/n}$. Extending the same idea, it is proposed to modify the equation to predict the plastic COD (Eq.(12)) as follows:

$$\delta_p = \alpha^{\frac{1}{n}} \varepsilon_y \pi R h_2 \left(\frac{M}{M_L}\right)^n \tag{17}$$

It will be shown in the next section that modifying these equations as shown in Eqs.(16-17) to predict the plastic *J*-integral and COD works excellently as long as fully plastic state is not attained. However, when fully plastic state is attained, Eqs.(16-17) significantly under-predicts the plastic *J*-integral and COD, which is non-conservative with respect to the prediction of crack initiation or maximum load. Probably, because of this, Zahoor did not persist with these modifications when he later published the Ductile Fracture Handbook (Zahoor, 1989-1991). The reason again lies with the material constitutive law. In the Ramberg-Osgood equation, the elastic strain (i.e. the first term of the right hand side of Eq.(2)) is dominant at initial loading and also in the transition region from elastic to fully plastic state. During this stage, Eqs.(11-12) over-predicts the plastic *J*-integral and COD, because, Eqs.(11-12) is appropriate (i.e. J_p, δ_p is proportional to α) when only plastic strain term is present in the Ramberg-Osgood equation or, in other words, Eq.(15) is used as material constitutive law. Therefore, use of Eq.(16-17) is appropriate during this initial loading stage as long as fully plastic state is not attained. However, in the fully plastic state, when, plastic strain becomes dominant and elastic strain becomes insignificant, Ramberg-Osgood equation (Eq.(2)) behaves more like Eq.(15) and Eqs.(11-12) predicts better the plastic *J*-integral and COD.

Consequently, it is recommended to use Eqs.(16-17) to evaluate the plastic *J*-integral and COD when $M/M_L \le 1$ and to use Eqs.(11-12) when $M/M_L \ge 1.2$. For $1 < M/M_L < 1.2$, to make the transition smoother, linear interpolation is done as follows:

$$J_p(1 < M/M_L < 1.2) = J_{p_1} + \frac{J_{p_{1.2}} - J_{p_1}}{0.2M_L}\left(M - M_L\right) \tag{18}$$

$$\delta_p(1 < M/M_L < 1.2) = \delta_{p_1} + \frac{\delta_{p_{1.2}} - \delta_{p_1}}{0.2M_L}\left(M - M_L\right) \tag{19}$$

where, J_{p_1} and δ_{p_1} are the plastic *J*-integral and COD evaluated at $M = M_L$ using Eqs.(16-17) and $J_{p_{1.2}}$ and $\delta_{p_{1.2}}$ are the plastic *J*-integral and COD evaluated at $M = 1.2 \times M_L$ using Eqs.(11-12). The elastic *J*-integral and COD are always calculated using the Eqs.(4-8). The next section discusses the experimental validation of these recommendations.

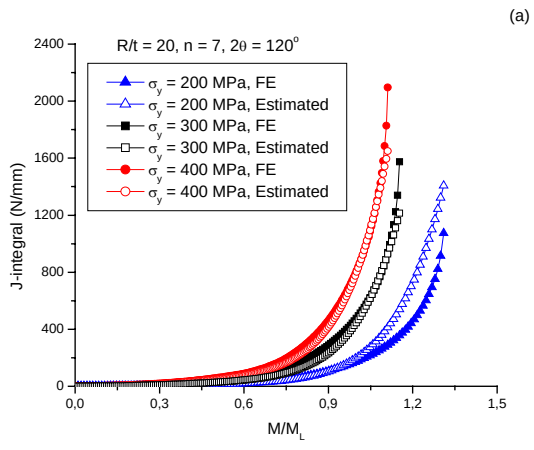

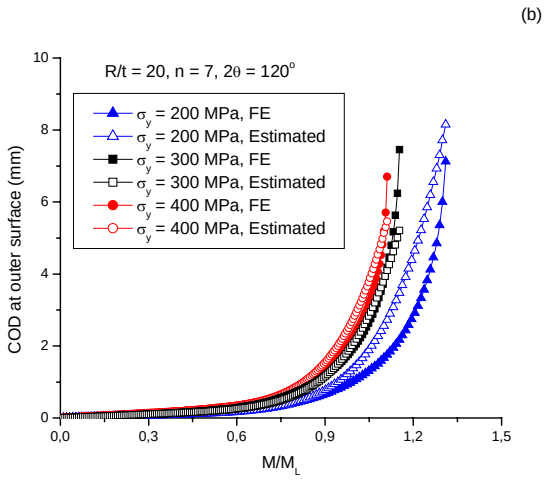

Fig.8 Effect of yield stress on (a) J and (b) COD-estimation scheme predictions

Figure 8 shows the effect of variation of yield stress on the *J* and COD estimation schemes. It compares the predictions of *J* estimation schemes with the finite element results with yield stress σ_y = 200 and 400 MPa in material constitutive equations (Eqs.(1-2)). A reasonably good matching may be observed. It should be noted that the plastic influence functions (h_1 and h_2), generated using σ_y = 300 MPa, are used to estimate *J* for yield stress σ_y = 200 and 400 MPa.

It may be noted here that the conventional GE/EPRI plastic zone correction of elastic J-integral, expressed as a function of strain hardening exponent (n), SIF and limit load is not recommended here. Because, its contribution has been found to be negligible up to the load range considered here and it makes the elastic *J* and COD estimation unduly complicated.

5. Effect of bend radius on proposed estimation schemes

As mentioned in section 3.1 and shown in Table 1, all the calculations, in general, have been done for long radius (R_b/R =3) elbows. However, few short radius elbows with R_b/R = 2 have also been analyzed to investigate the effect of bend radius on the proposed estimation schemes. The geometry constants (V_2 in Eq.(8)) to evaluate elastic COD at inside and outside surface and also the plastic influence functions i.e. h_1 for *J*-integral and h_2 for COD at inside and outside surface in Eqs.(11-12) are evaluated for various geometric cases and Ramberg-Osgood hardening index, n = 5. It has been observed that the V_2, h_1 and h_2 parameters are not same as obtained in case of long radius elbows (R_b/R = 3). However, it is also observed that the V_2, h_1 and h_2 parameters obtained for long radius elbows (R_b/R = 3) are at certain consistent ratios with respect to those parameters obtained for short radius elbows (R_b/R = 2). An average value of these ratios has been obtained by excluding few extreme cases and they are as follows:

V_2 for short radius elbow = V_2 for long radius elbow/1.259 (20)
(both inside and outside surface)

h_1 for short radius elbow = h_1 for long radius elbow/3.337 (21)

h_2 for short radius elbow = h_2 for long radius elbow/2.651 (22)
(both inside and outside surface)

6. Experimental validation

Any new *J* and COD estimation schemes need to be experimentally validated to gain confidence in it. It is easy to validate COD estimation schemes through direct comparison between predicted and experimentally measured values. However, in case of *J*-integral, one has to compare in an indirect way, that is, through comparison of crack initiation and unstable ductile tearing load. Crack initiation load is calculated based on $(J_i)_{SZW}$ and unstable ductile tearing load is calculated based on the tearing modulus approach (Paris et al, 1979) through the use of J-R curve. The $(J_i)_{SZW}$ is the initiation toughness (J_i) that is obtained from the stretched zone width (SZW) using ESIS P2-92, Appendix 4 (ESIS, 1992). The brief description of the elbow fracture experiments and the comparison between predictions of *J* and COD estimation schemes and test data are described below.

6.1 Brief description of elbow fracture experiment

As a part of comprehensive *Component Integrity Test Program*, fracture experiments were carried out by *Reactor Safety Division* of *Bhabha Atomic Research Centre* on ten elbows of 200 and 400 mm nominal bore diameter (NB) over the years 1999 – 2003. The elbows were having throughwall circumferential/axial cracks at elbow extrados/intrados/crown and subjected to closing/opening bending moment. However, out of total 10, only 4 fracture experiments on elbows with throughwall circumferential crack at extrados subjected to closing bending moment are of relevance here and described briefly. The complete details of these experiments are available in (Chattopadhyay et al, 2005, 2004b, 2004c). Table 4 shows the geometric details of the elbows. All the elbows are made of carbon steel (ASTM-A333Gr6) material. However, there are small differences of mechanical properties of 200 and 400 mm NB elbow materials because of heat-to-heat variation. Table 5 shows the mechanical properties of the 200 and 400 mm NB elbow materials.

Table 4 Details of Elbow Test Specimens

Test reference number	Mean bend radius (mm)	Outer diameter (mm)	Avg. wall thickness (mm)	Moment arm length* (mm)	Crack angles after fatigue pre-crack (2θ)
ELTWEX8-4	207	219	19.3	825.72	98.24^o
ELTWEX16-3	609	406	35.1	840.22	64.85^o
ELTWEX16-4	609	406	35.7	840.22	94.11^o
ELTWEX16-5	609	406	37.6	840.22	124.0^o

*Moment arm length is the perpendicular distance between the loading line and mid-section of elbow center-line for conversion of load to moment

Table 5 Mechanical Properties of SA 333 Gr 6 steel at Room Temperature

	200 mm NB elbow material	400 mm NB elbow material
Yield stress, σ_y	288 MPa	312 MPa
Ultimate tensile stress, σ_u	420 MPa	459 MPa
Young's modulus of elasticity, E	203 GPa	203 GPa
Percentage elongation	36.2	39.1
Percentage reduction in area	76.64	76.15
Poisson's ratio, ν	0.3	0.3
Ramberg-Osgood coefficient (α)with reference stress equal to yield stress	10.759	10.249
Ramberg-Osgood hardening exponent (n)	4.301	4.23
Initiation toughness, $(Ji)_{SZW}$	220 N/mm	236 N/mm

6.2 Comparison of test data with prediction

6.2.1 J-estimation

Table 6 compares the predicted crack initiation load with the test measurement. The prediction is made using the proposed *J*-estimation schemes as described in section 4 and also the finite element and R6 method (Option 2) as described in (Chattopadhyay et al, 2005). The $(J_i)_{SZW}$ based prediction of crack initiation load is done as follows:

$$J\,(a_o,P) = (J_i)_{SZW} \tag{23}$$

where, $J(a_o,P)$ is the applied *J*-integral calculated for initial crack size (a_o) as a function of load (P) either using the *J*-estimation schemes or the FEM and $(J_i)_{SZW}$ is used for respective elbow materials (see Table 5). Several investigations (e.g. Joyce and Link, 1997, Eisele et al, 1994, Pavankumar et al, 2002) have shown that $(J_i)_{SZW}$ is more or less independent of stress triaxiality and can be treated as an intrinsic material property. Hence, it is possible to predict the crack initiation loads by comparing $(J_i)_{SZW}$ determined from the laboratory specimen with the calculated crack driving force (applied J-integral) of the cracked component. Table 6 illustrates that in all the cases, the predicted crack initiation loads using the proposed *J*-estimation schemes are 8 – 15% conservative with respect to the test measurement, which is quite satisfactory.

Table 6 Comparison of crack initiation loads

Test no.	Expt. (kN)	Predicted crack initiation load (kN)		
		R6 (Chattopadhyay et al,2005)	FE (Chattopadhyay et al,2005)	Present estimation scheme
ELTWEX8-4	125	125.3	134	115 (8%)*
ELTWEX16-3	1360.4	1312.8	1249	1199 (11.9%)
ELTWEX16-4	995.5	991.3	989	849 (14.7%)
ELTWEX16-5	742.5	653.4	770	636 (14.3%)

*% difference = [(Expt.-predicted) × 100%]/Expt.

Regarding the prediction of unstable ductile tearing load, J-R curves obtained from small laboratory specimens having identical ligament constraint as that of the 200 and 400 mm NB elbows are used. Specimen J-R curves had to be extrapolated beyond test range to obtain the tangency condition between J-R curve and applied *J* versus crack length curves at a particular load. Three parameters power law fit is made to get the J-R curve equation in the test range, which is then extrapolated as required. This methodology was earlier (Pavankumar et al, 2003) shown to produce good results. The J-R curve equations used are as follows:

$$J_R = -462.465+1456.988(\Delta a)^{0.40527} \quad \text{(for 200 mm NB elbow material)} \quad (24)$$

$$J_R = -164.167+1421.6958(\Delta a)^{0.57382} \quad \text{(for 400 mm NB elbow material)} \quad (25)$$

(J_R in kJ/m^2 and Δa in mm and $\Delta a \geq 0.2$ mm)

Figure 9 shows the illustration of tangency condition for a typical elbow ELTWEX16-4. Table 7 shows the comparison of predicted unstable ductile tearing load/moment with the experimentally observed maximum load. A good matching is observed. In some cases where instability load is more than the maximum experimental load, it may happen that plastic collapse precedes the onset of unstable ductile tearing because of ovalisation of elbow cross section and very ductile nature of the material.

Table 7 Comparison of unstable ductile tearing load with the maximum test load

Test no.	Expt. maximum load (kN)	Predicted unstable ductile tearing load (kN)	Difference*
ELTWEX8-4	136	157	-15%
ELTWEX16-3	1387	1496	-8%
ELTWEX16-4	1275	1223	4%
ELTWEX16-5	976	1047	-7%

*% difference = [(Expt.-predicted load) × 100%]/Expt.

An exercise has also been carried out to compare the finite element *J*-integral for the real material (see Table 5) with the predictions of proposed J-estimation schemes for one typical tested elbow of 400 mm nominal diameter (test ref. no. ELTWEX16-4). Figure 10 shows the comparison. Total 4 methods of calculations are shown in the figure: i) Finite element calculation with actual material properties, ii) *J*-estimation scheme prediction using Eq.(11) for plastic component, iii) *J*-estimation scheme prediction using Eq.(16) for plastic component and iv) Recommended *J*-estimation scheme prediction i.e. elastic *J* calculation using Eq.(4-7) and plastic *J* calculation using Eq.(16) for $M/M_L \leq 1$, Eq.(11) for $M/M_L \geq 1.2$ and linear interpolation for $1 < M/M_L < 1.2$ using Eq.(18). The comparison is done only up to the maximum load because, the load controlled estimation scheme calculation cannot capture the drooping nature of load as in actual experiments. It shows that the calculation of elastic *J*-integral using Eq.(4) is quite accurate. Figure 10 also proves what has been mentioned in section 4, i.e. Eq.(16) is quite accurate to calculate the plastic *J*-integral up to almost $M/M_L \leq 1$, beyond which it under-predicts the plastic *J*-integral. The figure also shows that Eq.(11) over-predicts the plastic J-integral for $M/M_L \leq 1$. Finally, Fig.10 shows that the predicted J-integral using the recommended *J*-estimation schemes match quite satisfactorily with the finite element calculation for real material.

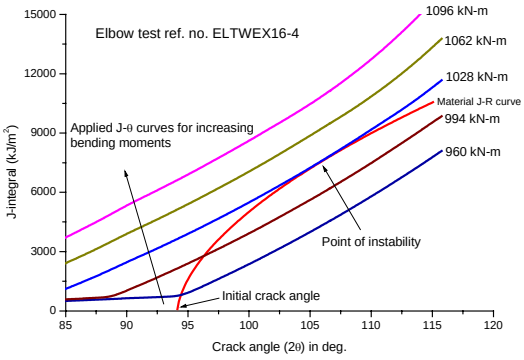

Fig.9 Determination of unstable ductile tearing load for one typical tested elbow ELTWEX16-4

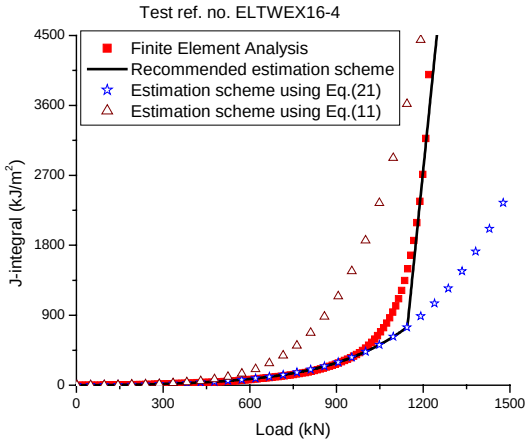

Fig.10 Comparison of J-integral for one typical tested elbow ELTWEX16-4

6.2.2 COD-estimation

Figures 11-14 show the comparison of experimental COD measured at outside surface of elbows with the prediction of estimation schemes. Three methods of calculations are shown in the figures: i) COD estimation scheme prediction using Eq.(12) for plastic component, ii) COD estimation scheme prediction using Eq.(17) for plastic component and iii) Recommended COD estimation scheme prediction i.e. elastic COD calculation using Eq.(8) and plastic COD calculation using Eq.(17) for $M/M_L \leq 1$, Eq.(12) for $M/M_L \geq 1.2$ and linear interpolation for $1 < M/M_L < 1.2$ using Eq.(19). Like J-integral, the comparison is again done only up to the maximum loadfor the same reason. All the figures show that calculation of elastic COD using Eq.(8) is quite accurate. It validates the accuracy of the proposed V_2 values given in Table 2. Regarding the calculation of plastic component of COD, the basic observation as made during comparison of *J*-integral holds true here also. Figures 11-14 prove that Eq.(17) is quite accurate to calculate the plastic COD up to almost $M/M_L \leq 1$, beyond which it under-predicts the plastic COD. The figures also show that Eq.(12) over-predicts the plastic COD for $M/M_L \leq 1$. Finally, Figs.11-14 illustrate that the predicted COD using the recommended COD estimation schemes match quite satisfactorily with the experimental measurements. It should be noted that elbow ELTWEX8-4 is a short radius elbow and hence eqns.(20-22) are used to calculate the V_2, h_1 and h_2 parameters. The other three are long radius elbows.

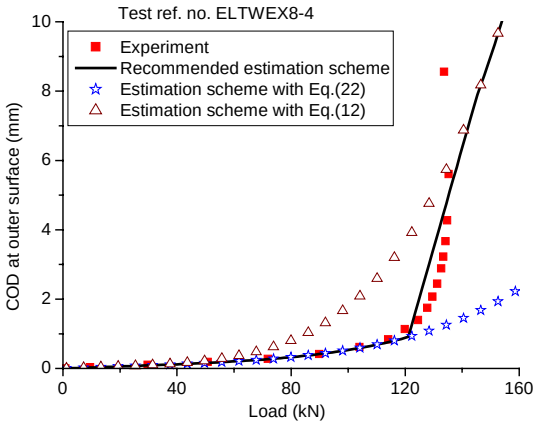

Fig.11 Comparison of COD for elbow no. ELTWEX8-4

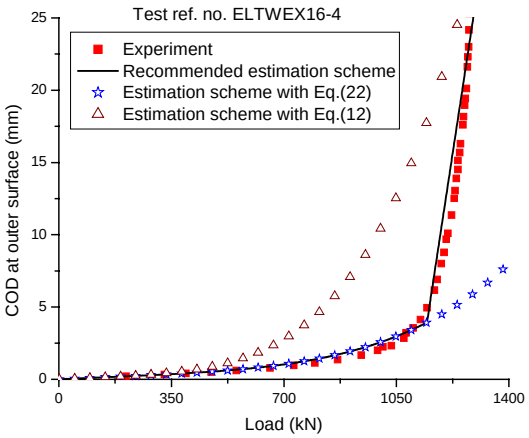

Fig.13 Comparison of COD for elbow no. ELTWEX16-4

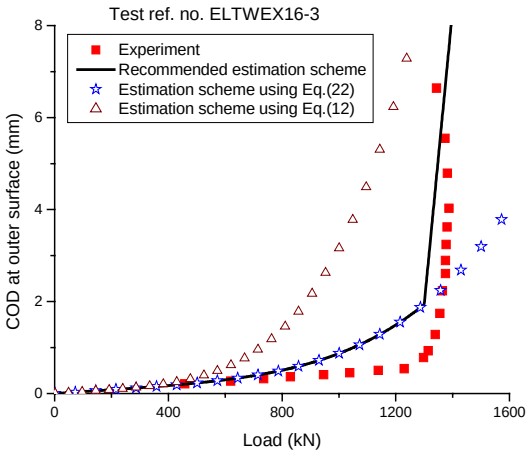

Fig.12 Comparison of COD for elbow no. ELTWEX16-3

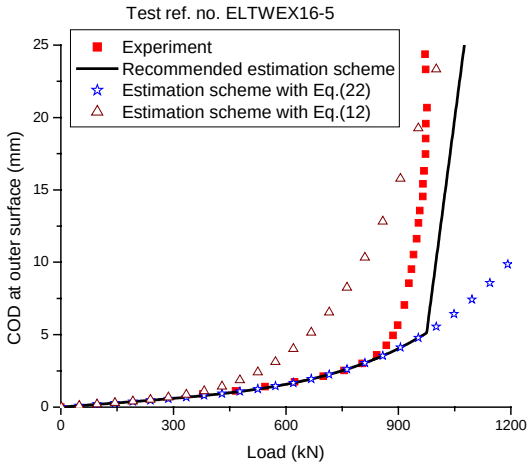

Fig.14 Comparison of COD for elbow no. ELTWEX16-5

7. Summary and Conclusions

Simple estimation schemes are proposed to evaluate elastic-plastic *J*-integral and COD of throughwall circumferentially cracked elbow subjected to closing bending moment. Non-linear finite element analysis of large number of elbows with wide ranges of geometric (R_b/R = 3, R/t = 5 – 20 and $2\theta = 45^o - 150^o$) and material parameters (n = 3,5,7) are carried out for the parametric study. Incremental flow theory of plasticity considering both material and geometric non-linearities is adopted to model the ovalisation of elbow cross sections during deformation, which significantly influences the elbow fracture behavior. Although it violates Ilyushin's (1946) theorem, however, it has been shown that the resulting estimation schemes are still reasonably accurate for engineering purpose. Experimental validation of proposed *J* and COD estimation schemes has been done by comparing the crack initiation and instability loads and COD. Numerical validation of *J*-estimation schemes has also been done by comparing the *J*-integral calculated through finite element analysis and predictions of proposed estimation schemes.

Reference

1. Brust, F.W., (1987), "Approximate Methods for Fracture Analysis of Throughwall Cracked Pipes", NUREG/CR-4583, United States Nuclear Regulatory Commission
2. Chattopadhyay,J., Dutta,B.K., Kushwaha,H.S., Mahajan,S.C. and Kakodkar,A., (1994), "A Database to Evaluate Stress Intensity Factors of Elbows with Throughwall Flaws under Combined Internal Pressure and Bending Moment", *Int. J. of Pres. Ves. and Piping*, **60**, pp 71 - 83
3. Chattopadhyay,J., Tomar,A.K.S., Dutta,B.K. and Kushwaha,H.S., (2004a), "Closed-form collapse moment equations of through wall circumferentially cracked elbows subjected to in-plane bending moment", *Journal of Pressure Vessel Technology*, ASME Transactions, **126,** pp 307-317
4. Chattopadhyay, J., Dutta B.K. and Kushwaha H.S., (2004b), "New 'η_{pl}' and 'γ' functions to evaluate J-R curves from cracked pipes and elbows: Part II –Experimental and numerical validation", *Engineering Fracture Mechanics*, **71**, pp 2661-2675
5. Chattopadhyay, J., Tomar,A.K.S., Dutta B.K. and Kushwaha H.S., (2004c), "Limit load of throughwall cracked elbows: Comparison of test results with theoretical predictions", *Fatigue and Fracture of Engg. Materials and Structures*, **27**, pp1091-1103
6. Chattopadhyay,J., Pavankumar,T.V., Dutta,B.K. and Kushwaha,H.S., (2005), "Fracture experiments on throughwall cracked elbows under in-plane bending moments : Test results and theoretical/numerical analyses", *Engineering Fracture Mechanics* , **72**, pp 1461 – 1497
7. Eisele, U., Herter, K.H. and Schuler X., (1994), "Influence of the multiaxility of stress state on the ductile fracture behavior of degraded piping components", ECF 10: Structural Integrity: Experiments, Models and Applications (Eds. Schwalbe, K.H., Berger C.), Berlin,1, pp 249 – 254.

8. ESIS, (1992), "ESIS procedure for determining the fracture behavior of materials", ESIS P2-92, Appendix 4, European Structural Integrity Society
9. Gullerud, K. Koppenhoefer, A.Roy, S.RoyChwodhury, M. Walters and R.H.Dodds, Jr., (2002), WARP3D–Release 14.0, 3–D Dynamic Nonlinear Fracture Analysis of Solids Using Parallel Computers and Workstations, University of Illinois, U.S.A.
10. Ilyushin,A.A., (1946), "The theory of small elastic-plastic deformations", *Prikadnaia Mathematika 1 Mekhanika*, **10**, pp 347 -353
11. Joyce, James A. and Link, Richard E., (1997), "Application of two parameter elastic-plastic fracture mechanics to analysis of structures", *Engineering Fracture Mechanics*, **57**, pp 431-436
12. Kim,Yun-Jae, Huh,Nam-Su, Park,Young-Jae, and Kim, Young-Jin, (2002), "Elastic-plastic *J* and COD estimates for axial through-wall cracked pipes", *International Journal of Pressure Vessel and Piping*, **79**, pp 451 - 464
13. Klecker,R., Brust,F.W. and Wilkowski, G.M., (1986), "NRC Leak-Before-Break Analysis Method for Circumferentially Throughwall Cracked Pipes Under Axial Plus Bending Loads", NUREG/CR-4572, United States Nuclear Regulatory Commission
14. Kozluk,M.J., Manning,B.W., Misra,A.S., Lin,T.C., and Vijay,D.K., (1988), "Linear elastic solutions for long radius piping elbows with curvilinear throughwall cracks", in *Advanced Topics in Finite Element Results*, Cory,J.F., and Gordon,J.L., Editors, ASME PVP-Vol.143, The American Society of Mechanical Engineers, pp 23-28
15. Kumar,V., German,M.D., and Shih,C.F., (1981), "An Engineering Approach for Elastic-Plastic Fracture Analysis", EPRI-NP-1931, Project 1287 - 1, Topical Report, Electric Power Research Institute, Palo Alto, CA
16. Kumar,V., German,M.D. and Shih,C.F., (1983), "Elastic-plastic and fully plastic analysis of crack initiation, stable growth and instability in flawed cylinders", *Elastic-Plastic Fracture : Second Symposium, Volume I – Inelastic Crack Analysis, ASTM STP 803,* C.F.Shih and J.P.Gudas, Eds., American Society for Testing and Materials, pp I-306 – I-353
17. Kumar,V., German,M.D., Wilkening, Andrews,W., deLorenzi,H., and Mowbray,D., (1984), "Advances in Elastic-Plastic Fracture Analysis", EPRI-NP-3607, Final Report, Electric Power Research Institute, Palo Alto, CA
18. Kumar,V., and German,M.D., (1988), "Elastic-plastic fracture analysis of throughwall and surface flaws in cylinders", EPRI-NP-5596, Electric Power Research Institute, Palo Alto, CA
19. Mohan,R., Krishna,A., Brust,F.W., and Wilkowski,G.M., (1998), "*J*-estimation schemes for internal circumferential and axial surface cracks in pipe elbows", *Journal of Pressure Vessel Technology*, ASME Transactions, **120**, pp 418-423
20. NISA, (2002), Customized Pre-processor for A General Purpose Finite Element Program, *Engineering Mechanics Research Corporation*, Michigan, USA
21. Novtech Corporation, (1988), "Evaluation of flaws in ferritic piping", EPRI-NP-6045, Final Report, Electric Power Research Institute, Palo Alto, CA
22. Paris, P.C., Tada, H., Zahoor, A. and Ernst, H., (1979), "The Theory of Instability of the Tearing Mode of Elastic-Plastic Crack Growth", *Elastic-Plastic Fracture*, ASTM STP 668, J.D.Landes, J.A. Begley and G.A. Clarke, Eds., American Society for Testing and Materials, Philadelphia, pp 5-36
23. Pavankumar, T.V., Chattopadhyay, J., Dutta B.K. and Kushwaha H.S., (2002), "Transferability of specimen J-R curve to straight pipes with throughwall circumferential flaws", *International Journal of Pressure Vessels and Piping*, **79,** pp127-134.
24. Pavankumar, T.V., Chattopadhyay, J., Dutta B.K. and Kushwaha H.S., (2003), "Role of stress triaxiality (q) in assessing fracture behavior of cracked components", 29th MPA Seminar, Oct. 9 & 10, MPA, University of Stuttgart, Germany
25. Piping Review Committee, (1984), "Evaluation of potential for pipe breaks", NUREG/CR-1061, Vol.3, US Nuclear Regulatory Commission, Washington DC
26. Rahman,S., and Brust,F.W., (1992) , "An estimation method for evaluating energy release rates of circumferential throughwall cracked pipe welds", *Engineering Fracture Mechanics*, **43**, pp 417 – 430
27. Shih,C.F., Moran,B., and Nakamura,T., (1986), "Energy release rate along a three-dimensional crack front in a thermally stressed body" *International Journal of Fracture*, **30**, pp 79 – 102
28. Zahoor,A., (1987), "Evaluation of J-integral estimation schemes for flawed throughwall pipes", *Nuclear Engineering and Design*, **100**, pp 1-9
29. Zahoor,A., (1989 – 1991), "Ductile Fracture Handbook", Vol.1-3, EPRI-NP-6301-D, N14-1, Research Project 1757-69, Electric Power Research Institute

